Submitted for "Identification of Existing and Emerging Microelectromechanical Systems (MEMS) Applications" session, sponsored by committee A2F09

Design and Testing of a MEMS Ultrasonic Transducer for Flaw Detection

Irving J. Oppenheim, Akash Jain, and David W. Greve
Carnegie Mellon University

ABSTRACT

Ultrasonic pulse-echo methods are versatile, effective procedures for inspecting welds in steel structures. However, the ultrasonic methods conventionally used have two disadvantages: inspection must be performed manually by a skilled technician, and the signal obtained at the time of one inspection provides no "memory" to be used at the time of a later inspection. Our research involves the development of MEMS ultrasonic flaw detection devices that could be permanently installed at critical locations, that would maintain a history of earlier signal characteristics, and that would be polled remotely. One purpose of this paper is to acquaint researchers with the development of MEMS devices, and another is to present experimental results demonstrating the feasibility of our approach for MEMS ultrasonic flaw detection in solids. We first outline the fabrication choices afforded to developers of such devices, and then describe the design decisions made in developing our device. We next describe results of electrical characterization, again using our chip and our experimental study of its electromechanical properties as a case study. We then describe the experiments we performed to establish chip performance as a detector of ultrasonic signals, with particular interest in its performance as a phased array transducer to localize a signal source. We report successful demonstration of signal detection and source localization, and conclude that a MEMS ultrasonic transducer can perform phased array signal detection in contact with solids.

Contact information

Irving J. Oppenheim (corresponding author), Department of Civil and Environmental Engineering, Carnegie Mellon University, Pittsburgh, PA 15213, Telephone 412-268-2950, Fax 412-268-7813, email ijo@cmu.edu.
Akash Jain, Department of Electrical and Computer Engineering, Carnegie Mellon University, Pittsburgh, PA 15213, email akash@andrew.cmu.edu.
David W. Greve, Department of Electrical and Computer Engineering, Carnegie Mellon University, Pittsburgh, PA 15213, Telephone 412-268-3707, Fax 412-268-2860, email dg07@andrew.cmu.edu.

INTRODUCTION

Motivation

Bridge girders are inspected visually, but ultrasonic examination would be a more reliable and more informative alternative. If ultrasonic examination can be made less expensive than visual inspection, then both improved technical performance and reduced cost could be achieved. Our goal is to develop MEMS ultrasonic devices to monitor conditions at critical locations in steel bridge girders or truss members. The devices would be affixed during erection and would function indefinitely without external power supplies or other connections. The devices would perform sensing and signal interpretation, and would report their findings remotely.

The concept is to build an ultrasonic flaw detection system on a chip using a MEMS (microelectronic mechanical systems) device as a receiver array with, a mm-scale piezoelectric element (part of the chip packaging) as the ultrasonic source. The system is intended to scavenge power from structural strains and to report results with fly-by polling using RF communications. The concept requires the development of phased array signal processing, and/or signature analysis signal processing, to perform flaw detection (flaw imaging) from the fixed location of a resident transducer. The overall concept is a major innovation in instrumented flaw detection and monitoring, and is a paradigm shift when compared to non-instrumented methods such as visual inspection.

Background: Ultrasonic Flaw Detection

Ultrasonic flaw detection is a versatile technology, and Figure 1 depicts the principle of the pulse-echo method, taken from Krautkramer (*1*). An ultrasonic pulse is emitted into the material and reflects from the first boundary it encounters. The time elapsed between the emission of the pulse and the reception of the echo, multiplied by the speed of sound in the medium, corresponds to twice the distance between the transducer and the boundary. For a plate with no flaws the boundary would be the back surface, in which case the method would measure the plate thickness. Such thickness-gauging is useful in many applications, including the assessment of section loss from corrosion. An internal flaw as depicted in Figure 1 would be evidenced as a premature echo, in which case the method would measure the depth to the flaw. In current practice, an operator estimates the size of the flaw by sweeping the region over which the echo is detected. Of course, the case illustrated in Figure 1 is oversimplified, and users of ultrasonic flaw detection often encounter and recognize multiple flaws, weld porosity, and other pertinent conditions.

Present ultrasonic flaw detection practice is memoryless, taking no advantage of the earlier signal history, whereas a resident flaw detection system would be a perfect candidate to use that history for signature analysis or for a record of flaw growth. However, there are several major challenges to using a MEMS transducer for ultrasonic flaw detection. It is necessary to scan a relatively large area from the fixed position of a resident transducer, and therefore a MEMS transducer must function as a phased array, providing the distance and orientation to any source.

A piezoelectric material such as PZT can work effectively as both emitter and receiver. However, a MEMS transducer is not expected to perform well as an emitter into steel for reasons to be discussed elsewhere in this paper. In the work described here, we chose to use a PZT element as the emitter and to develop a MEMS transducer as the phased receiver array for signal detection.

Previous work

The principles of ultrasonic pulse-echo detection are used in many other applications including medical ultrasound imaging, and there is a considerable history of research into MEMS transducers, mostly for fluid-coupled and air-coupled applications. The investigators' approach to microscale ultrasonic diaphragm design was based on the important earlier work of Khuri-Yakub at Stanford University (*2,3,4,5*). Reference (*2*) outlines the mechanical and electrical analysis of capacitive diaphragm transducers and presents experimental results for air-coupled and fluid-coupled transmission through aluminum, showing that practical applications (including flaw detection) are feasible. Reference (*3*) records in detail the fabrication steps needed to produce capacitive ultrasonic transducers suitable for immersion applications and the characterization, both experimental and analytical, of their performance. Reference (*4*) presents results for nondestructive evaluation of metal specimens, in which air-coupled transducers generate and receive Lamb waves, which are useful for detecting near-surface flaws. Reference (*5*) discusses one-

dimensional detector arrays and presents initial imaging results, in which solids immersed within fluids are detected. Other investigators of MEMS ultrasonics are Schindel, whose work (*6*) presents experimental results and comparisons to theory for immersed transducers, and Eccardt, whose work (*7*) includes the demonstration of devices combining MEMS structures and semiconductor electronics.

APPROACHES TO MEMS DESIGN AND FABRICATION

Semiconductor electronic devices are fabricated by a series of steps such as material deposition, lithographic definition, and etching, which are typically repeated in sequence to create multiple layers. A process consists of an established sequence of such steps, in which the material properties and the thickness of each layer are fixed. MEMS structures are often fabricated by similar steps, but it is useful to distinguish among different approaches for fabrication of MEMS devices. We can distinguish four different approaches:

- Custom process development: The most sophisticated MEMS devices are typically fabricated using custom processes that have been developed to construct mechanical structures with preferred material types and dimensions, together with the supporting semiconductor electrical circuits.
- Adaptation of an existing multi-user semiconductor process: In a multi-user process many designs are grouped together onto the silicon wafer, which is then diced to return the individual devices to their designers. For example, a typical wafer may have a diameter of 15 cm, and a user may purchase a die as small as 2 mm square. There exist several multi-user processes for the fabrication of semiconductor devices, each featuring a fixed process sequence with published design rules. One approach to developing MEMS devices is to use some portion of the die area to construct mechanical structures, typically using metal, insulator, and polysilicon layers as structural materials, while the other portion of the die area contains the electrical circuits. This adaptation of a semiconductor process requires postprocessing to release the mechanical structures.
- A multi-user process for MEMS structures and supporting electrical circuits: Such a process would be the ideal environment for researchers to use in developing MEMS devices, but no such commercial process provides multi-user access at the present time.
- A multi-user process for MEMS mechanical structures: One multi-user process exists, namely the MUMPs process.

The MUMPs process (*8*) contains three layers of polysilicon deposition and surface micromachining, and is derived from a process first developed at Berkeley. An insulating nitride layer is deposited on the silicon substrate, followed by three polysilicon layers (Poly-0, Poly-1, and Poly-2) separated by two sacrificial oxide layers.

DEVICE DESIGN

We made the conceptual design decision to fabricate a linear phased array using the MUMPs process to make diaphragm type transducers with a natural frequency (in air) near 4 or 5 MHz. Khuri-Yakub *(2)* has shown that a capacitive-type MEMS device approaches the performance of PZT as an emitter only when operated at very small gaps, and therefore in our design the phased array functions as the receiver while conventional PZT materials are used for the excitation. Our design was completed within five months, including graduate student training, approximate engineering analysis, and CAD layout. In this section we discuss some of the detailed design decisions.

Configuration of an Individual Diaphragm

The basic unit is a capacitor with a stationary plate constructed in poly-0 and a flexible plate, or diaphragm, constructed in poly-1, separated by the gap created when the oxide layer is removed by a chemical release. Following Khuri-Yakub *(2)*, our design calculations were based upon circular plates which were then approximated for fabrication with hexagonal plates; however, square plates would have equally been a suitable design choice. Figure 2 depicts the plan and section of the typical hexagonal diaphragm unit in our design. The poly-1 layer has a thickness of 2 microns, an elastic modulus of 180 GPa, Poisson's ratio of 0.25, and a specific gravity of 2.30. We simplified the analysis by assuming an equivalent circular diaphragm with rigid (fixed) supports. Under those assumptions, a natural frequency

near 5 MHz was predicted for a diaphragm with a diameter near 85 microns. We chose the leg length of the hexagonal diaphragm to be 49 microns, which inscribes a circle with an approximate diameter of 85 microns.

With reference to the plan and section views in Figure 2, the elements of the typical diaphragm and its fabrication are discussed below:

- The stationary plate of the capacitor is the innermost hexagon in the plan view. It has a leg length of 37.5 microns and is fabricated in the poly-0 layer, which has a thickness of 0.5 microns. Electrical contact to that plate is made by forming a conductor, approximately 10 microns wide, exiting to the south in the plan view.
- The anchor for the diaphragm appears in plan as the incomplete hexagonal polyline, outside of the stationary plate, with a leg length of 49 microns and a width of approximately 20 microns. The anchor structure bears upon the poly-0 layer and is the poly-1 layer deposited through the anchor mask. The anchor is connected to the diaphragm, structurally and electrically.
- The anchor structure is incomplete along its southern edge to allow passage of the conductor from the stationary plate, which is necessary to isolate the two plates of the capacitor from one another. The elements are spaced apart from one another by 7 microns. Similarly, a clear spacing of 7 microns is maintained in the poly-0 layer between the stationary plate and the anchor. We note that the spacing between such elements can in principle be reduced to a MUMPs design rule strict minimum of 4 microns or recommended minimum of 5 microns. However, in designing this first-generation device we chose to be conservative and used a 7 micron spacing, because one electrical short would render a whole detector useless.
- The space between the stationary plate and the diaphragm is the oxide-1 layer, which is a sacrificial layer of 2 micron thickness. This layer is removed during the etching process to create a structure (the diaphragm) elevated from the substrate with a gap of 2 microns.
- The diaphragm itself is the largest hexagon with a leg length along the anchor structure of 49 microns. Per MUMPs design rules, the diaphragm contains etch holes of 5-micron size spaced 30 microns apart; the etch holes are required for removal of the sacrificial oxide-1 layer by an acid etch process.

The mask layout drawings for an individual diaphragm were prepared, and then were repeated to create the larger structure of a detector.

Configuration of a Typical Detector

A single diaphragm would have a capacitance of only 0.016 pF, whereas a target capacitance of several pF was considered a necessary minimum. Therefore, each detector was to be constructed as a large number of diaphragms in parallel. In principle, large detectors would have been the most sensitive. However, two other considerations governed the size of an individual detector. One consideration was the need to fabricate an array of multiple detectors for phased array operation. The second consideration was the need to limit the individual detector to a dimension less than or roughly equal to the signal wavelength. We chose to build a detector containing 180 diaphragms, with a predicted capacitance of 2.9 pF. The detector is approximately 0.9 mm wide and 2 mm long, and its layout is shown in Figure 3. .

Configuration of the Overall Chip

In one MUMPs run a user acquires 15 copies of a die with a size of 1 cm square, which can be subdiced to dimensions as small as 2.5 mm. For example, a user constructing a small device, less than 5 mm square, could replicate the design four times on their die, could subdice each chip into four subchips, and could therefore obtain 60 devices from a single run. However, in our design the device makes use of the full die area, for two major reasons. We sought a long baseline for the phased array, sufficient to accommodate a large number of detectors; the nominal length of 1 cm corresponds to multiple wavelengths of the ultrasonic signal and admits the placement of nine detectors along its length. We also decided to perform most experiments in a probe station, which requires exposing a portion of the perimeter for contact by the probes. The nominal length of 1 cm allows most of the chip to be placed into contact with our test specimens, while leaving exposed the one edge containing the contact pads.

Figure 4 is the layout drawing for the overall chip. The primary array is the column of nine detectors at the east, the contact pads form the column of 48 small rectangles at the extreme west, and the conductor paths between them are plainly visible. (The column just east of center is an array of nine detectors using

an alternate diaphragm design, and the column just west of center is a set of objects prepared for possible physics experiments. Results presented in this paper are obtained from the primary array at the east.)

Numerous detailed design decisions are associated with the layout plan. For example, the life of a device is often governed by damage at its contact pad; probing deforms the pad and repeated probing eventually causes a mechanical breach of the insulating nitride layer and a short-circuit. Other design tradeoffs concern the number of detectors on the chip, the size of the contact pads, and the amount of chip area lost to the conductor paths.

ELECTRICAL CHARACTERIZATION

Measurements were made to obtain the electrical properties of the device, to determine whether the expected mechanical behavior was present, and to permit the comparison of predicted and measured performance. In this particular research effort two types of tests were performed: capacitance-voltage measurements and admittance measurements. The device was placed in a probe station, in which the user makes contact with selected conductor pads using two micromanipulator probes.

Capacitance-Voltage Measurements

An undeflected diaphragm is a parallel plate capacitor which then changes capacitance with deflection. For parallel plates the capacitance C is calculated as $A\varepsilon_o/d$, where A is the plate area, ε_o is the permittivity of free space, and d is the gap between the plates. The capacitance of an individual detector was measured as a function of applied bias voltage using an HP-4280A 1-MHz capacitance meter, using a bias voltage varying from -100 to +100 V and a probe voltage of 30 mV. A representative plot of capacitance as a function of bias voltage, C(V), is shown in Figure 5, along with a best-fit parabola which corresponds to the equation $C=5.29\cdot10^{-12} + 1.71\cdot10^{-18}\,V^2$, with C in farads and V in volts.

A bias voltage on the plates of a capacitor produces an attractive force between the plates. In this case one plate is a diaphragm, which deflects under such an attractive force. Using small-displacement assumptions, the capacitance is predicted to vary with the square of the bias voltage. Therefore, the measurement of a parabolic C(V) is evidence that the diaphragms behave as expected.

More detailed examination of these results involves comparing the measured and the predicted coefficients. The capacitance of the detector under zero bias voltage can be calculated as the parallel capacitance of 180 hexagons with a leg length of 37.5 microns and a gap of 2.0 microns. The predicted capacitance is 2.9 pF, which is considerably less than the measured capacitance of 5.29 pF. However, stray capacitances are always present; sources for stray capacitance include the capacitance between the conductors and the substrate, capacitance through the anchor structures, capacitance through the conductor paths, and so on. Moreover, in this first design little attention was given to minimizing such stray capacitances. Therefore, the higher capacitance observed in testing was not unexpected, and we interpreted it as a measure of stray capacitance.

The coefficient describing the change in capacitance with V^2 was predicted from a structural mechanics model, although a number of simplifying assumptions were utilized, such as replacing the hexagonal diaphragm with an equivalent circular diaphragm. The structural boundary conditions were not known with certainty, and therefore calculations were performed using the two limits of simply supported and rigidly supported boundaries. The predicted coefficients were $1.7\cdot10^{-18}$ and $0.32\cdot10^{-18}$, respectively, and we considered the measured coefficient of $1.71\cdot10^{-18}$ to be consistent with that predicted range. (In our opinion it was only a coincidence that the coefficient predicted for the simply-supported case is identical to the measured coefficient.)

C(V) measurements were obtained for all nine detectors, with little variation from one to another, as would be expected. The symmetrical results in Figure 5 are for the case of an unbonded detector, free to deflect. Other measurements were made for detectors glued into contact with solids, and as expected those C(V) measurements displayed a stiffer, asymmetrical, hysteretic behavior.

Admittance Measurements

The basic diaphragm was designed to have a fundamental structural vibration frequency near 5 MHz. An HP-4192 impedance analyzer was used to measure admittance (current/voltage) as a function of frequency in the range from 100 kHz to 6 MHz, using an applied bias voltage together with a probe voltage of 1 V. It was expected that the structure would vibrate when excited electrically at its fundamental

frequency and therefore display a change in admittance, and the test would serve to measure that frequency and the damping characteristics.

We were unsuccessful in our initial attempts to observe a resonance in the admittance measurements, but we were confident from our C(V) measurements that the diaphragm was behaving as an elastic structure, and that it would demonstrate a fundamental vibration frequency largely as expected. We hypothesized that the resonance under ambient conditions was not sufficiently sharp to be easily detected from the admittance results, and that a much sharper resonance would be observed in a vacuum. However, our probe station was not suitable for placement within a vacuum chamber. Therefore, we mounted a device in a ceramic package, which required the additional step of wire-bonding between the contacts on the chip and the contacts on the ceramic package. When that step was completed, the device was placed within a vacuum chamber and the admittance measurements were repeated, and a resonance at 3.47 MHz was observed. Figure 6 shows the admittance near the resonant frequency in five different experiments. The admittance was measured at four different pressures -- 0.0, 0.29, 0.61, and 1.0 atmosphere -- at a constant bias voltage of 35 V; the admittance was also measured at 0.0 atmosphere with zero bias voltage.

The admittance measured at 35 V bias voltage and 0.0 atmosphere shows multiple peaks, which are absent in the measurements obtained at higher pressures. We note that our detector consists of 180 hexagonal diaphragms in parallel with some variation in their boundary conditions; consider the difference between one diaphragm along an edge and another diaphragm contained within the interior. We attribute the multiple peaks to the slight differences in fundamental frequency associated with boundary conditions. In the presence of greater damping, with increased air pressure, those peaks are no longer recognizable.

The fundamental frequency for a hexagonal diaphragm can be calculated. Structural boundary conditions were not known with certainty, and therefore calculations were performed using the two limits of simply supported and rigidly supported boundaries, predicting frequencies of 2.5 MHz and 4.5 MHz, respectively. The measured frequency, of 3.47 MHz, is consistent with such a bounding analysis.

Figure 6 shows the resonant frequency to increase slightly with air pressure. We attribute the shift in resonant frequency to additional stiffness contributed by the air trapped beneath the diaphragm. Calculating that stiffness from Boyle's law, assuming that the air is perfectly trapped and that the temperature does not change, leads to a predicted 1.1% increase in resonant frequency between 0.0 and 1.0 atmosphere, whereas we measured a 0.46% increase. However, air is not perfectly trapped beneath the diaphragm because some air can escape from the etch holes, and therefore we expect the shift to be less than that calculated from Boyle's law. In our opinion, the comparison between the predicted and measured increase in resonant frequency is reasonable.

The sharpness of resonance decreases with pressure as a result of the damping contributed by the presence of air. In vacuum we measured a Q factor (the electrical engineering term for the dynamic magnification at resonance) of 910, which we interpret to reflect internal damping in the structure, and at atmospheric we measured a Q of 49.6, reflecting the additional damping provided by the air. We identified two mechanisms by which the presence of air would contribute damping and thereby lessen the Q. One is the radiation of ultrasonic energy into the air, for which we calculated a predicted Q of 230, and another is squeeze-film damping, for which we developed a simplified bounding model (not shown) and calculated a predicted Q of 29, for a combined predicted Q of 26. In our opinion, the comparison between the predicted and measured change in damping is reasonable.

We considered it important to conduct a control experiment by performing admittance measurements with zero bias voltage; those data points plot as the diagonal line in Figure 6. Under zero bias voltage a diaphragm-type transducer should display negligible mechanical response to a voltage excitation, even at its resonant frequency, which is confirmed by the data in Figure 6. This finding constitutes evidence that the response recorded in the other experiments in Figure 6 is the result of transducer mechanical function. Similarly, the admittance measurements were repeated at different bias voltage levels because the response is predicted to be linear with bias voltage, a fact which was confirmed experimentally.

EXPERIMENTAL RESULTS, PHASED ARRAY SIGNAL DETECTION

Experiments were performed using aluminum, brass, and plexiglass test specimens. Figure 7 depicts the test specimen used to demonstrate phased array signal detection. The device was bonded to a plexiglass specimen using Gelest Zipcone CG silicone adhesive, and a commercial transducer with a nominal diameter of 15 mm and an operating frequency of 3.5 MHz was mounted to the specimen as the signal source. The baseline of nine detectors appears as the heavy line in Figure 7, with a distance of 18 mm

(0.72 in) between the signal source and the nearest detector. The signal reaches the nine detectors at an extreme raking angle, 65^o away from the normal, with considerable variation in arrival time predicted across the array of nine detectors. The purpose of the test was to obtain the distance from the transducer to the source, and the orientation angle, in the plane as pictured, using phased array signal processing.

The assembly was placed in a probe station, which allowed measurements to be made from only one detector at a time. Therefore, the experiment was performed separately for each detector and the results were combined retrospectively. A Krautkramer USPC-2100 generated the excitation at a period of 2 milliseconds, and an oscilloscope was used to record the signal at the detector, averaging 256 times.

Figure 8 shows the experimental results, where the abscissa for each detector signal has been placed along the ordinate at a position proportionate to its geometric location along the array. Only seven signals are shown, because two detectors had become non-operative during the course of the experiments. The signal arrives first at the closest detector and shows a delay of approximately 310 nanoseconds in its arrival time at successive detector locations. The arrival time establishes the distance between the source of the pulse and any detector, and the delay between detectors permits angular localization of the source. A simple geometric interpretation can be envisioned directly on Figure 8. If a vertical line is drawn through the pulses at the start of each record, and a diagonal line is drawn through the points marking the receipt of the signal at each detector, the lines will intersect at a position that can be scaled (either from the baseline dimension or from the inter-detector spacing) to obtain the distance projected along the plane of the device, from which the angle of 25^o (or the off-normal angle of 65^o) can be calculated.

The results of a numerical approach to phased array signal processing, described fully in reference *(9)*, are shown in Figure 9. There exist only two unknowns for signal localization -- distance from the source to midpoint of the array, and orientation angle between the source and the plane of the array. We calculate a time shift between successive detectors as a simple geometric function of the distance and orientation, we then add all seven shifted signals, and finally we record the amplitude of the summed signal. If the individual signals are shifted by the proper interval, then the amplitudes will add coherently to yield a maximum signal. Figure 9 (plotted with arbitrary units) depicts the results of that process with distance read on the axis projecting into the foreground and orientation angle read on the complementary axis. The isolated peak represents the best estimate of the distance and orientation between the source and the array; the peaks along the distance axis are artifacts of stray electrical coupling.

DISCUSSION

The work described herein represents approximately 15 months of effort. The device design and layout was completed in the first five months, culminating in the submission of the CAD files for fabrication, and the subsequent fabrication time was approximately two months. Initial electrical characterization studies, and the initial demonstration of ultrasonic signal detection in a thickness-gauging geometry, occupied the next three months. The admittance measurements in vacuum and interpretation of characterization results were performed in approximately two months. The experiments in phased array signal processing and the preparation of results required approximately three months. These were our first efforts, and therefore much of the calendar time was spent in devising specimens, establishing the measurement methods, responding to emerging problems such as excessive stray capacitance or imperfect grounding, iterating and improving on initial measurement efforts, checking results for repeatability, performing control experiments, and so on. We subsequently designed other devices for related applications and observed a much-shortened schedule because of our prior experience and re-use of methods. For example, we can report the recent design and layout of a comparable device (fabricated in the MUMPs process) within two months, and the electrical characterization of that new device in approximately one month.

The results demonstrate that a MEMS diaphragm-type detector array can localize an ultrasonic signal source. However, effective flaw detection will require detection of small reflected signals, which is a more challenging problem. One approach envisioned is to use a mm-scale PZT specimen as a source producing a spherical waveform, and then to interpret the signals (the echoes) arriving at the detector array in order to image the flaw boundary from which the echoes reflect. Among the many challenges in doing so, we observe that the acoustic intensity of echoes from the small spherical source will be smaller, by orders of magnitude, than the acoustic intensity employed in our experiments to-date. The sensitivity of our detector array is insufficient to undertake such experiments. While we have achieved considerable improvement in sensitivity using a suitable amplifier, we cannot overcome the stray capacitance and unwanted coupling in our current configuration using off-chip electronics. However, if our device were to be fabricated with on-

chip electronics, then we expect to see an improvement in sensitivity sufficient to undertake these additional experiments. In our opinion the MUMPs process was an ideal method for designing and fabricating the prototype transducer, but our work has now reached the stage where an integrated device, combining electromechanical detectors with electronics for signal processing, is needed.

CONCLUSIONS

We have described our design and testing of a MEMS transducer used for phased array detection of ultrasonic signals in solids. We show electrical characterization measurements that are in reasonable agreement with predicted behavior, and we demonstrate successful source localization using simple processing of phased array signals. We offer the demonstration as proof-of-concept that a MEMS transducer can be fabricated and can detect ultrasonic signals when glued into contact with solids. We directly show successful thickness-gauging, and we offer the successful localization results as evidence that phased array signal processing, which will be necessary for scanning or imaging, has been achieved. We suggest that multi-user processes, like the MUMPs process used here, be considered by other research teams seeking to address the development of transducers for civil infrastructure applications.

ACKNOWLEDGEMENTS

This work was supported by the Pennsylvania Infrastructure Technology Alliance program, funded by the Commonwealth and administered at Carnegie Mellon by the Institute for Complex Engineered Systems, and by gifts from Krauktramer Ultrasonic Systems, which the authors gratefully acknowledge.

REFERENCES

1. Krautkramer, J. and Krautkramer. H., *Ultrasonic Testing of Materials*, 4th edition, Springer Verlag, Berlin, 1989.
2. Ladabaum, I., Jin, X., Soh, H., Atalar, A., and Khuri-Yakub, B., "Surface micromachined capacitive ultrasonic transducers," *IEEE Trans. On Ultrasonics, Ferroelectrics, and Frequency Control*, Vol. 45, 678-690, 1998.
3. Jin, X., Ladabaum, Degertkin, F., Calmes, S., and Khuri-Yakub, B., "Fabrication and characterization of surface micromachined capacitive ultrasonic immersion transducers," *IEEE Jnl. Of Microelectricmechanical Systems*, Vol. 8, 100-114, 1999.
4. Hansen, S., Mossawir, B., Ergun, A., Degertkin, F., and Khuri-Yakub, B., "Air-coupled nondestructive evaluation using micromachined ultrasonic transducer," *IEEE Ultrasonics Symposium*, 1037-1040, 1999.
5. Oralkan, O., Jin, X., Kaviani, K., Ergun, A., Degertkin, F., Karaman, M., and Khuri-Yakub, B., "Initial pulse-echo imaging results with one-dimensional capacitive micromachined ultrasonic transducer arrays," *IEEE Ultrasonics Symp.*, 959-962, 2000.
6. Bashford, A., Schindel, D., and Hutchins, D., "Micromachined ultrasonic capacitance transducers for immersion applications," *IEEE Trans. On Ultrasonics, Ferroelectrics, and Frequency Control*, Vol. 45, 367-375, 1998.
7. Eccardt, P., Niederer, K., Scheiter ,T., and Hierold, C., "Surface micromachined ultrasound transducers in CMOS technology," *IEEE Ultrasonics Symp.*, 959-962, 1996.
8. Koester, D., Mahadevan, R., Hardy, B., and Markus, K., *MUMPs Design Handbook*, Cronos Integrated Microsystems, Research Triangle Park, NC, 2001.
9. Oppenheim, I., Jain, A., and Greve, D., MEMS ultrasonic transducers for the testing of solids," *IEEE Trans. On Ultrasonics, Ferroelectrics, and Frequency Control*, in press, 2002.

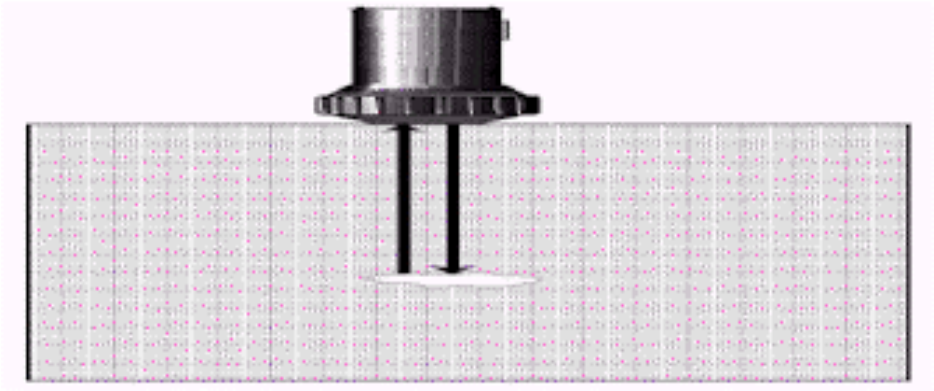

Figure 1. Principle of pulse-echo flaw detection from Krautkramer (*1*)

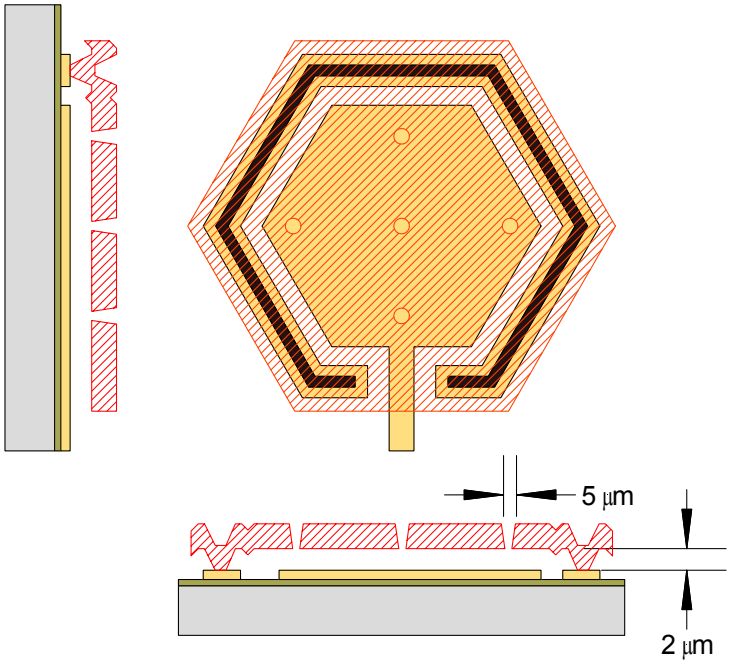

Figure 2. Sketch of typical diaphragm unit

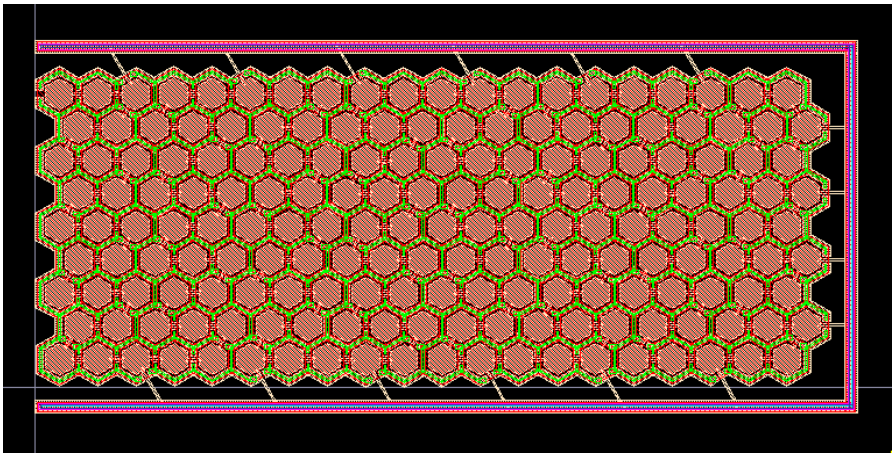

Figure 3. Typical detector, approximately 0.9 mm x 2 mm, containing 180 diaphragm units

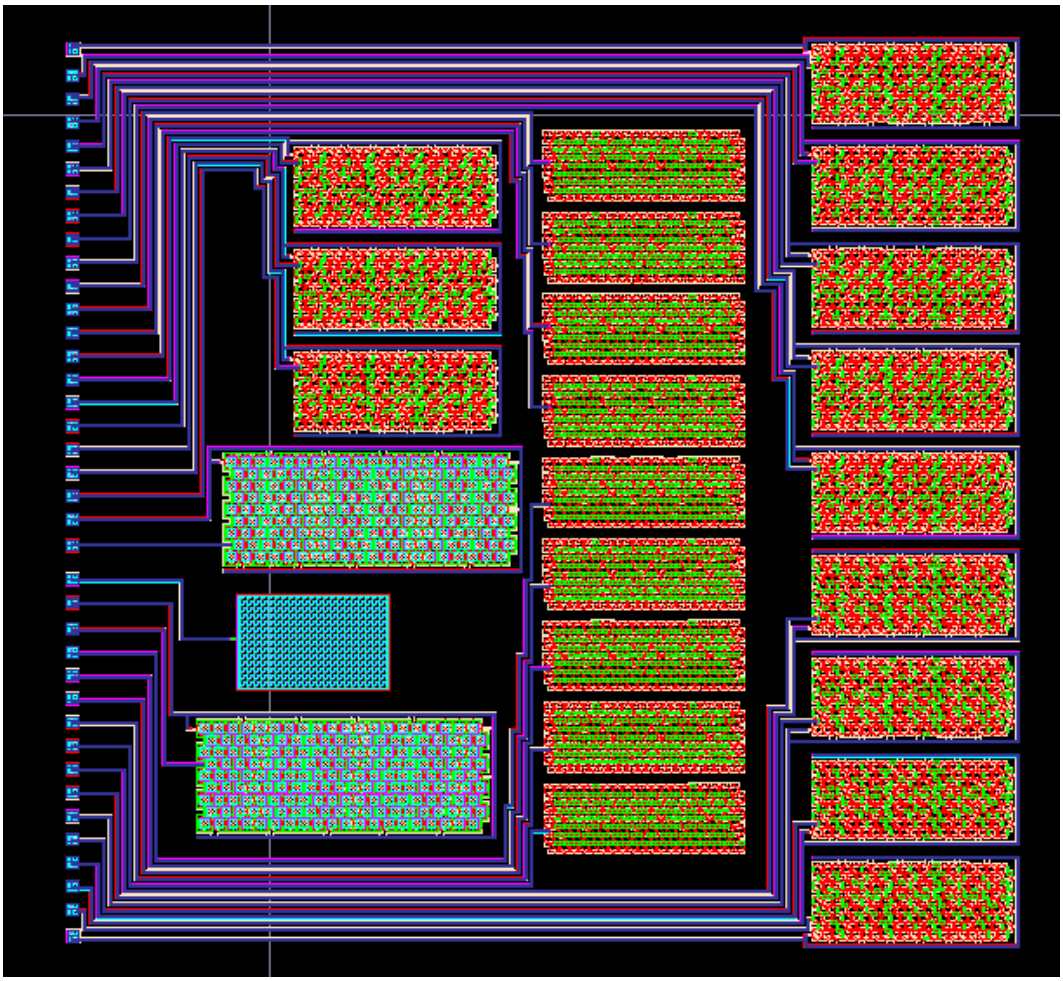

Figure 4. CAD layout drawing of chip, 1 cm x 1 cm, array of nine detectors at right

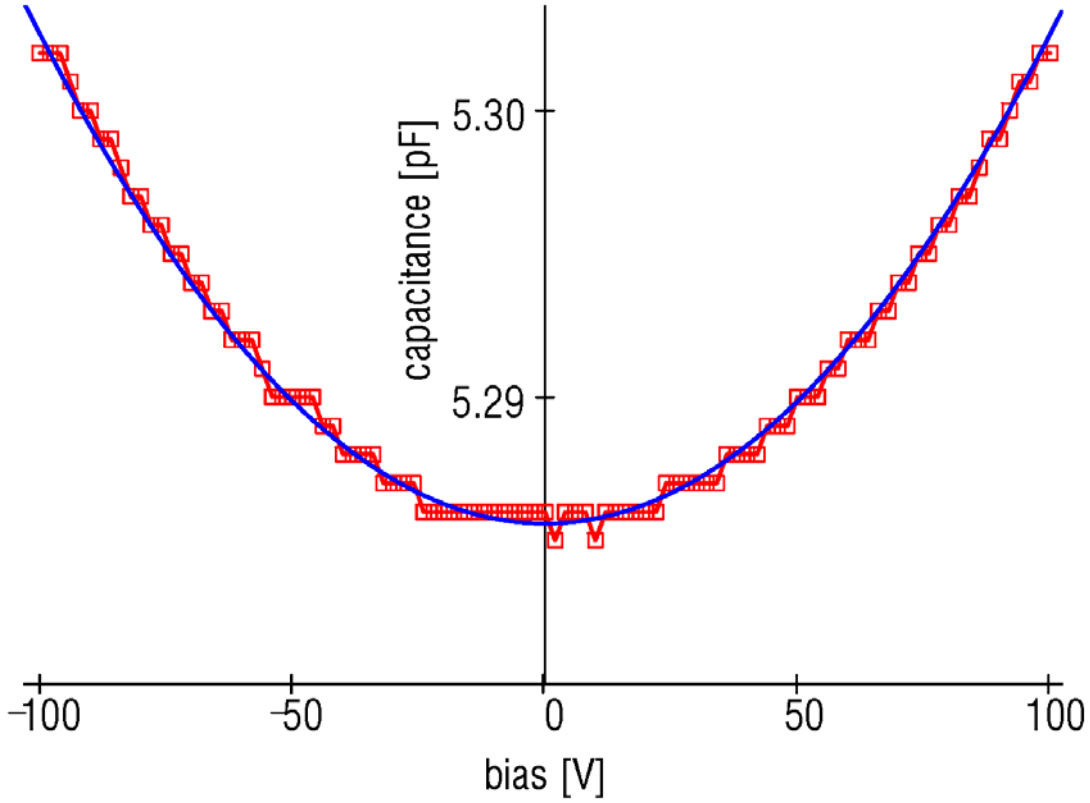

Figure 5. Measurements of capacitance v. voltage; experimental data and parabolic fit

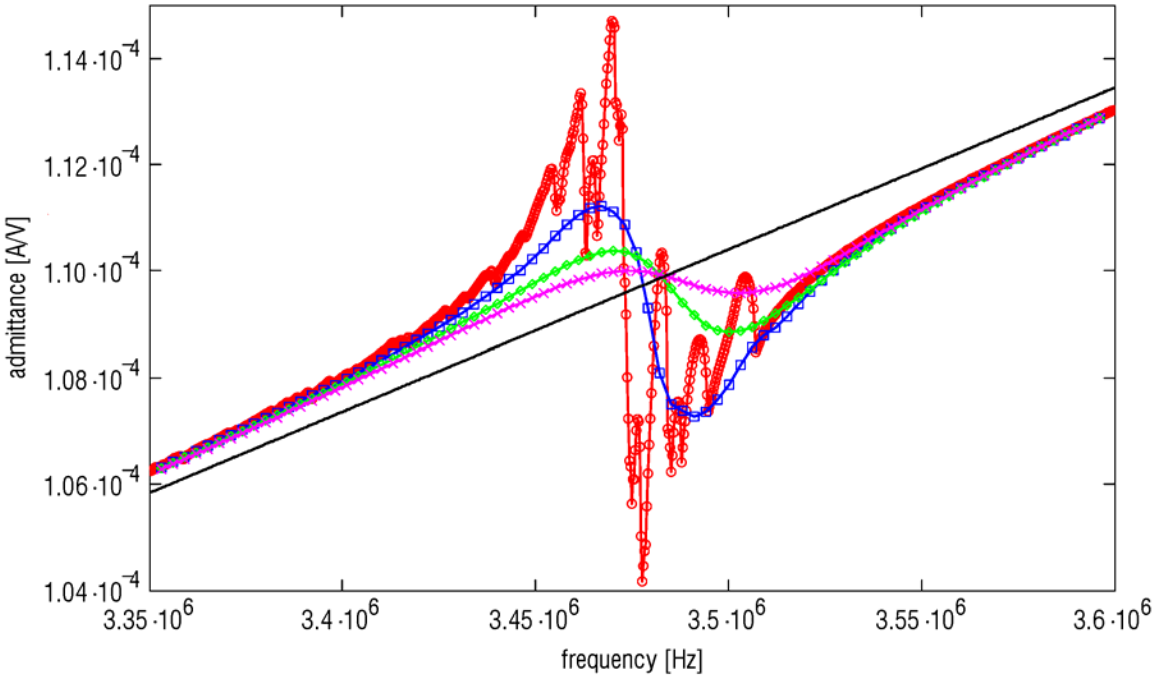

Figure 6. Admittance measurements with 35 V bias at 0 atm (o), 0.29 atm (□), 0.61 atm (◊), 1 atm (x); admittance measurements with 0 V bias at 0 atm (solid line).

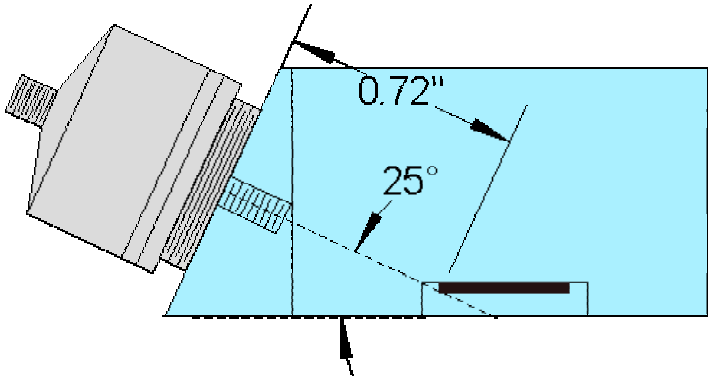

Figure 7. Test specimen for phased array experiments

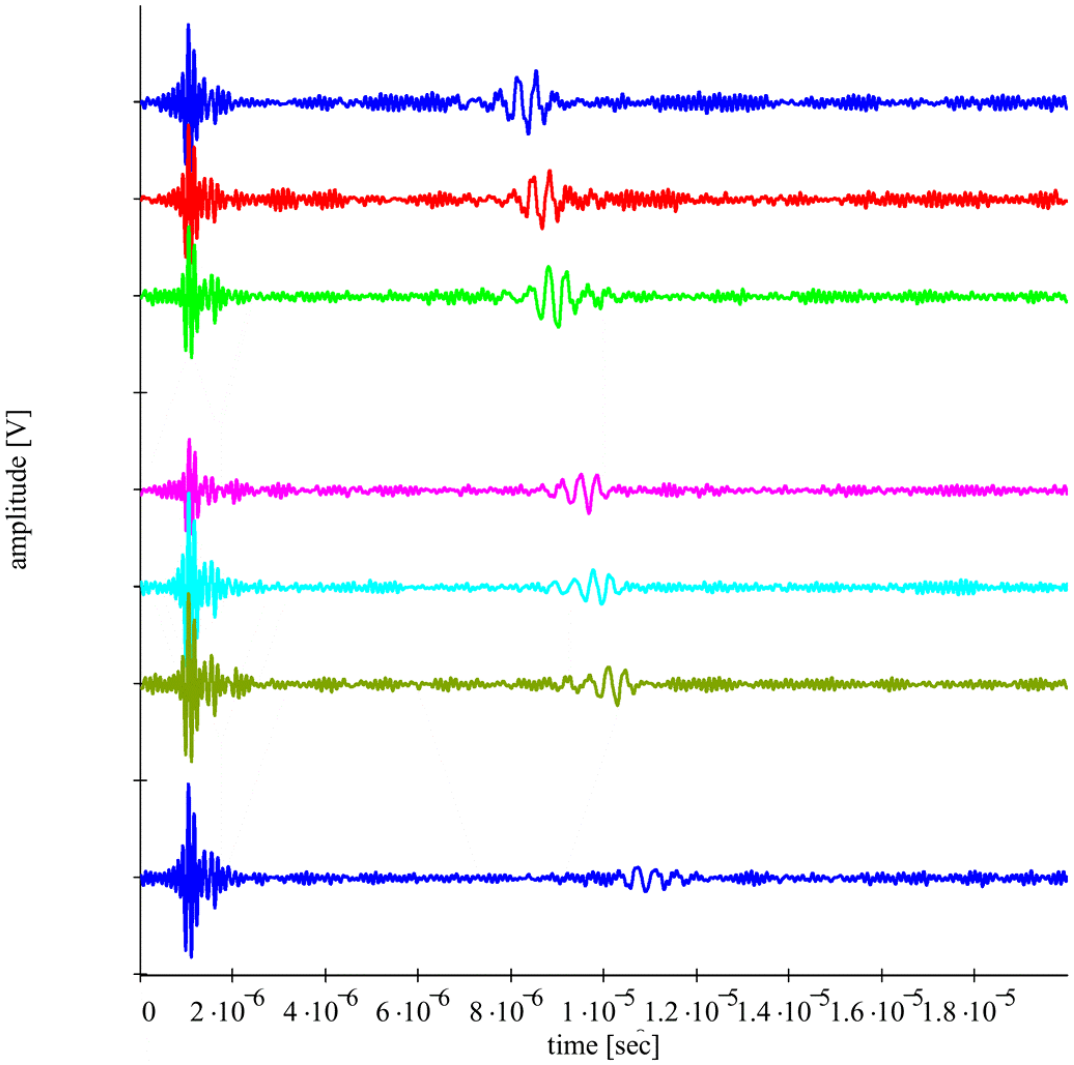

Figure 8. Experimental results, signals received at detector locations along the array

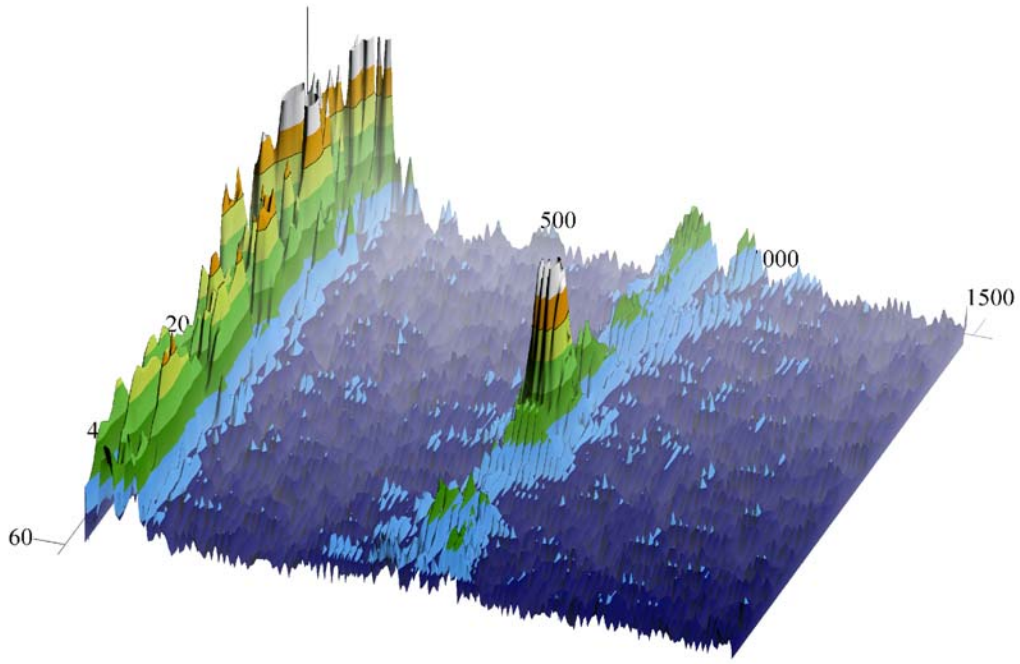

Figure 9. Phased array signal processing, peak corresponding to distance and orientation angle